

## Fluidisation characteristics of granular activated carbon in drinking water treatment applications

Kramer, O.J.I.; van Schaik, C.; Dacomba Torres, P.D.R.; de Moel, P.J.; Boek, E.S. ; Baars, E.T.; Padding, J.T.; van der Hoek, J.P.

**DOI**

[10.1016/j.appt.2021.06.017](https://doi.org/10.1016/j.appt.2021.06.017)

**Publication date**

2021

**Document Version**

Final published version

**Published in**

Advanced Powder Technology

**Citation (APA)**

Kramer, O. J. I., van Schaik, C., Dacomba Torres, P. D. R., de Moel, P. J., Boek, E. S., Baars, E. T., Padding, J. T., & van der Hoek, J. P. (2021). Fluidisation characteristics of granular activated carbon in drinking water treatment applications. *Advanced Powder Technology*, 32(9), 3174-3188. <https://doi.org/10.1016/j.appt.2021.06.017>

**Important note**

To cite this publication, please use the final published version (if applicable). Please check the document version above.

**Copyright**

Other than for strictly personal use, it is not permitted to download, forward or distribute the text or part of it, without the consent of the author(s) and/or copyright holder(s), unless the work is under an open content license such as Creative Commons.

**Takedown policy**

Please contact us and provide details if you believe this document breaches copyrights. We will remove access to the work immediately and investigate your claim.



Original Research Paper

# Fluidisation characteristics of granular activated carbon in drinking water treatment applications



O.J.I. Kramer<sup>a,b,c,d,f,\*</sup>, C. van Schaik<sup>c,d</sup>, P.D.R. Dacomba-Torres<sup>a,c</sup>, P.J. de Moel<sup>a,e</sup>, E.S. Boek<sup>f</sup>, E.T. Baars<sup>c</sup>, J.T. Padding<sup>b</sup>, J.P. van der Hoek<sup>a,c</sup>

<sup>a</sup> Delft University of Technology, Faculty of Civil Engineering and Geosciences, Department of Water Management, PO Box 5048, 2600 GA Delft, the Netherlands

<sup>b</sup> Delft University of Technology, Faculty of Mechanical, Maritime and Materials Engineering, Department of Process and Energy, Leeghwaterstraat 39, 2628 CB Delft, the Netherlands

<sup>c</sup> Waternet, PO Box 94370, 1090 GJ Amsterdam, the Netherlands

<sup>d</sup> HU University of Applied Sciences Utrecht, Institute for Life Science and Chemistry, PO Box 12011, 3501 AA Utrecht, the Netherlands

<sup>e</sup> Omnisys, Eiberlaan 23, 3871 TG Hoevelaken, the Netherlands

<sup>f</sup> Queen Mary University of London, Division of Chemical Engineering, School of Engineering and Materials Science, Mile End Road, London E1 4NS, United Kingdom

## ARTICLE INFO

### Article history:

Received 1 April 2021

Received in revised form 12 June 2021

Accepted 17 June 2021

Available online 27 July 2021

### Keywords:

Drinking water treatment

Liquid-solid fluidization

Granular activated carbon

Green-based materials

Expansion characteristics

Porosity prediction modelling

## ABSTRACT

Granular activated carbon (GAC) filtration is an important unit operation in drinking water treatment. GAC filtration is widely used for its filtration and adsorption capabilities as a barrier for undesired organic macro- and micro-pollutants. GAC filtration consists of two successive phases: adsorption and filtration, capturing the impurities from the water in conjunction with a backwash procedure in which the suspended particles are flushed out of the system. Available literature predominantly focusses on adsorption. A less frequently discussed but nevertheless equally crucial aspect of this operation is the backwash procedure of GAC beds. To prevent accumulation of suspended particles and to avoid additional operation costs, optimal backwashing is required. Another factor is sustainability: water utilities are showing increasing interest in exploring new sustainable GAC media. As these have different bed expansion tendencies due to different GAC characteristics with varying geometries, operational developments are needed for prediction models to estimate the expansion degree during backwashing. The prediction of the bed expansion of GAC is complex as the particles are non-spherical, porous and polydisperse. Through a combination of advanced particle laboratory and fluidisation experiments, we demonstrate a new approach which leads to an improved expansion prediction model for the backwashing of GAC filters.

© 2021 The Society of Powder Technology Japan. Published by Elsevier B.V. and The Society of Powder Technology Japan. This is an open access article under the CC BY license (<http://creativecommons.org/licenses/by/4.0/>).

Subscripts, superscripts and abbreviations can be found in the [Supplementary material](#) (Section 8)

## 1. Introduction

Granular activated carbon (GAC) filtration is widely applied in advanced drinking water treatment plants for its filtration and adsorption capabilities as a barrier for undesired macro- and micro-pollutants [1,2,3]. Increasing levels of organic micro-pollutants (OMP) in surface water used as source for drinking water production have led water supply companies in the

Netherlands to integrate activated carbon technologies in their drinking water treatment plants [4]. GAC is regenerated every 1–3 years to destroy the adsorbed components contained on its surface. The GAC filtration process consists of two successive phases. During the filtration and adsorption phase, suspended solids and dissolved organics are removed from the water through filtration and adsorption, respectively. Accumulation of suspended solids increases the head loss. When a head loss setpoint is exceeded, the accumulated particles are removed from the GAC filter during the backwash phase through an up-flow water stream and additional air scouring. For reliable and safe drinking water production, a precise specification of backwash rates for filter cleaning is needed. Therefore, robust and flexible treatment processes require thorough design specifications and process control of backwash rates for filter cleaning [5,6]. Regarding GAC filtration, the scientific literature focusses mainly on the adsorption capacity of GAC

\* Corresponding author at: Delft University of Technology, Faculty of Civil Engineering and Geosciences, Department of Water Management, PO Box 5048, 2600 GA Delft, the Netherlands.

E-mail addresses: [onno.kramer@waternet.nl](mailto:onno.kramer@waternet.nl), [o.j.i.kramer@tudelft.nl](mailto:o.j.i.kramer@tudelft.nl) (O.J.I. Kramer).

## Nomenclature

### Symbols

$D$	Inner column or cylinder vessel diameter [m]
$d_p$	Effective or average or particle equivalent diameter [m]
$d_{s,i}$	Sieve mesh diameter [m]
$d_{i,max}$	Maximum diameter (minor axis of ellipse) [m]
$d_{i,min}$	Minimum diameter (minor axis of ellipse) [m]
$E$	Bed expansion [%]
$g$	Local gravitational field of earth equivalent to the free-fall acceleration [m/s <sup>2</sup> ]
$L$	Fluid bed height [m]
$L_0$	Fixed bed height [m]
$m_{meas}$	Submerged SSD particle mass weighed under water [kg]
$m_{od}$	Mass of particles dried in oven [kg]
$m_{op}$	Mass of internal open pores [kg]
$m_{sub}$	Submerged SSD particle mass [kg]
$m_{ssd}$	Particle mass at saturated surface condition [kg]
OPV	Open pore volume [L/kg]
$\Delta P_{max}$	Total maximum differential pressure over the bed [kPa]
$Q_w$	Water flow [m <sup>3</sup> /h]
$v_s$	Linear superficial velocity or empty tube fluidisation velocity [m/s]
$V$	Volume [m <sup>3</sup> ]
$V_{ext}$	Volume of the external voids (outside) between particles [m <sup>3</sup> ]

$V_{bulk}$	Bulk volume, GAC particles including external voids [m <sup>3</sup> ]
$V_{op}$	Open pore volume (entirely wetted) [m <sup>3</sup> ]
$V_p$	Volume of porous particles (solid and internal pores) [m <sup>3</sup> ]
$V_{tp}$	Volume of total pores (open and closed internal pores) [m <sup>3</sup> ]
$V_s$	Skeletal carbon volume with closed pores [m <sup>3</sup> ]

### Greek symbols

$\varepsilon$	External porosity (voidage) system [m <sup>3</sup> /m <sup>3</sup> ]
$\varepsilon_0$	External fixed bed porosity [m <sup>3</sup> /m <sup>3</sup> ]
$\varepsilon_{mf}$	External porosity (voidage) at minimum fluidisation [m <sup>3</sup> /m <sup>3</sup> ]
$\eta$	Dynamic fluid viscosity [kg/m/s]
$\nu_T$	Kinematic fluid viscosity [m <sup>2</sup> /s]
$\rho_{bulk}$	Bulk density [kg/m <sup>3</sup> ]
$\rho_f$	Fluid density [kg/m <sup>3</sup> ]
$\rho_p$	Particle density [kg/m <sup>3</sup> ]
$\rho_s$	Skeletal density [kg/m <sup>3</sup> ]
$\rho_{wet}$	Wet density [kg/m <sup>3</sup> ]
$\rho_w$	Water density [kg/m <sup>3</sup> ]

[7–12] and less on the backwashing insights and challenges posed by filters.

Although significant progress has been made in recent decades towards the accurate prediction of the expansion of uniform, non-porous and spherical media [13], limited work has been published on the fluidisation characteristics of polydisperse, non-spherical and porous GAC grains in water. Due to the growing importance of GAC filtration in the field of water treatment, a thorough understanding of the expansion behaviour of GAC facilitates the ability to improve the accuracy of bed expansion predictions. Operational constraints of the GAC filters, such as the degree of bed expansion and particle bed stratification, are determined by the water temperature, water flow, GAC particle size, density, shape and size distribution. Consequently, the accurate prediction of the expansion degree of GAC beds is complex. To cope with fluctuations and variations, full-scale GAC filters are commonly over-designed [5]. To meet sustainability goals [14–16], water companies are exploring the use of more sustainable raw materials for drinking water treatment. Traditionally, GAC is manufactured from coal, but the use of sustainable materials [17] such as coconut shells and wood, is gaining popularity. Due to the differences in raw materials and manufacturing processes, different GAC granules also have different particle properties. Therefore, the transition to alternative GAC media also has implications for the process control of GAC filters, both in the filtration phase and in the backwashing phase. Changing GAC media can lead to two main operational problems: media washout and solids accumulation. If backwash velocities are too high, media washout is likely to happen. This results in high economic losses for water companies. If backwash velocities are too low, solids accumulation or the formation of mud balls can occur. This not only affects the filter performance, but it also leads to increased backwashing operations such as a higher frequency, again resulting in increased operational expenses. Another problem with fluidisation of GAC is that the particle size distribution (PSD) might adversely affect the water quality. GAC filters need to be stratified [3,18] to prevent the movement of

contaminant-saturated GAC particles to lower parts of the bed, which increases the risk of being desorbed and thus the risk of compromising the effluent of this treatment process. Understanding the fluidisation behaviour of porous media, and GAC in particular, can substantiate the decision of water companies to switch to more sustainable materials. Therefore, the need for knowledge about the GAC fluidisation behaviour is of major importance.

Scientific papers, with some dating back as far as to the 1920s [19–22], were originally derived specifically for spherical particles to describe the hydraulic behaviour of fluid flows through packed or fluidised beds. These models were often used to describe the hydraulic behaviour of non-spherical particles on the basis of particle shape correction factors intended to describe the particle's morphology through sphericity, surface area to volume ratios or other types of correlations using spheres. *De facto*, the granular media involved in water treatment processes, and especially GAC media, are non-spherical. Several experimental investigations concerning activated carbon fluidisation and particle size distributions have been performed. Experimental data presented by van Lier [23] revealed that the different models applied to describe the fluidisation behaviour of different GAC types performed well only for specific carbon types and conditions. Similarly, findings reported by Akkoyunlu [24] show that the proposed models, based on the Richardson–Zaki model, seem to fit well but also had limitations in terms of accuracy and application. Dabrowski [25] proposed empirical models to predict the media expansion for specific GAC types assuming that the fluidisation velocity is inversely proportional to the water viscosity. The prediction accuracy increased when the model was corrected for temperature, depending on the type of commercial carbon that was analysed. Sholji [26]; Trussell and Chang [27]; Clements and Haarhoff [28]; Ujhidy et al. [29] studied the expansion of filter media with Carman–Kozeny or Ergun-like equations using shape factors and model modifications to fit the experimentally obtained data or to improve the prediction accuracy. More recently, Nikam [30] used an Ergun-based approach to study the fluidisation of GAC particles, albeit in a

gas-solid fluidised bed. Hoyland [31] proposed a general model applicable to granular fixed and fluidised beds based on fundamental hydrodynamics for porous beads, based on the hydraulic conductivity approach of Carman–Kozeny. No detailed information was provided about the voidages of the examined particles, so it is unclear if this model is suitable for porous beads such as GAC. Hunce et al. [32] and Hunce et al. [13] carried out accurate fluidisation experiments with porous media and laboratory experiments to obtain the particle and skeletal densities. For the expansion prediction, they used a specific drag relation based on similar Ergun and Carman–Kozeny principles. More recent research used computational fluid dynamics (CFD) modelling to study the behaviour of non-spherical particles: Cornelissen et al. [33]; Zhang et al. [34]; Samstag et al. [35]; Blais and Bertrand [36]; Mema and Padding [37]; Cahyadi et al. [38] applied CFD for GAC media. Despite the academic insights reported in these works, neither effective voidage prediction models were proposed, nor thorough information was shared regarding scrutinised GAC particle properties. Still, this information is crucial to be able to describe the fluidisation behaviour of GAC in filter backwashing for water treatment processes.

In general, there is no agreement which model is the most adequate for describing the fluidisation characteristics, *i.e.* bed voidage, of irregularly shaped, polydisperse and porous media in liquid–solid fluidisation processes. It is common practice to use shape factors to correct for particle diameters to improve numerical results. In addition, regarding GAC grains, there is no consistent procedure detailing how to cope with the wide range of fixed bed porosities at minimum or incipient fluidisation. The *classical* models are based on fixed bed and incipient porosities for rigid spherical particles with porosity values around 0.4. The porosities for GAC media at minimum or incipient fluidisation are in general considerably higher, with values between 0.50–0.65 [2]. This is caused by the irregular shape combined with large particle size distribution of GAC media. During fluidisation, the bed stratifies: the large particles migrate to the bottom region of the bed and the smaller particles to the top of the bed [39]. Since these large and small particles are then no longer mixed, the voidage will be determined by packing of highly irregular particle shapes and therefore relatively higher than for more spherical particles. The voidage, however, is relatively unstable, *i.e.* it is the loosest possible configuration and can decrease considerably under the influence of external factors [40]. This voidage can be determined by fluidising the GAC filter bed and then allowing the particles to settle gradually. The minimum fluidisation point thus gives crucial information (starting point) for determining the backwash operation [41]. The influence of the backwash on voidage is crucial and needs to be considered when measuring this variable, *i.e.* minimum fluidisation velocity and voidage [39,3].

Regarding fixed bed and incipient voidage of porous GAC, there is no agreement in the scientific literature either. Worch [42] mentioned fixed bed porosities between 0.35–0.40. Sholji [26]; Knezev [43] found similar values between 0.38–0.42. Velten [10] and Clements [39] found slightly higher values for several GAC types between 0.39–0.52 and van Lier [23] measured fixed bed porosities for several GAC types between 0.58–0.62, which is in line with values reported in the standard work by Crittenden et al. [2], and Chowdhury et al. [12] gave more general values between 0.5–0.8. Regarding minimum fluidisation porosities, Nikam and Mandal [30] presented incipient porosities between 0.40 and 0.45. Pushnov [44] mentioned the dependency of the fixed bed voidage on the ratios of the vessel to the grain diameter and the shape of the grains. This had already been found by Ergun [21] for incipient porosities. In many publications considering filter backwashing, the degree of bed expansion as a function of the bed height:  $E = L/L_{mf} - 1$  is used instead of the voidage:

$L/L_{mf} = (1 - \varepsilon_{mf})/(1 - \varepsilon)$ . This is most likely because operational GAC filters are typically expanded for  $25\% < E < 30\%$  for 20–30 min with a main focus on bed heights and a smaller focus on porosities [41]. To our knowledge, no model exists that accurately describes the fluidisation behaviour of activated carbon grains that differ in particle size, PSD, shape and morphology and that have low particle-to-fluid density. The classical hydraulic models in the reviewed literature provide limited applicability for irregularly shaped media with high incipient porosities, which limits their applicability. The present study seeks to close the knowledge gap regarding the fluidisation behaviour of activated carbon grains for drinking water production applications.

The aim of this research was to gain insight into the fluidisation behaviour and the relation with characteristics of granular activated carbon grains applied in water treatment processes. This was done by performing advanced laboratory measurements, conducting hydraulic multiphase flow experiments and exploring the possibility of modelling the voidage using classical models as well as empirical data-driven models based on symbolic regression. The following factors with regard to the expansion characteristics of GAC were investigated:

- Particle size and shape: high degree of non-sphericity, large polydispersity.
- Particle density: due to the porous character of GAC media, multiple densities can be defined based on the packing and wettability on the rate of imbibition and adsorption of constituents from the water phase.
- Particle behaviour: particle orientation and re-arranging and changing drag.
- Particle change: attrition due to abrasive character of the bed during repetitive backwashing as well as particle growth due to biological activity.

For an extensive exploration, nine different GAC types were examined with a wide variety of grain size, particle shape, degree of polydispersity and raw materials.

This work focuses on the liquid–solid fluidisation. Air scouring is not taken into consideration.

## 2. Materials and methods

### 2.1. Particle selection – a wide variety in properties and sources

For this research, nine different GAC samples were selected and analysed as presented in Table 1. The GAC types can be divided into three different categories: spherical (*balls*), non-spherical (*granular or rock-like*) and extruded (*rod-like*). An example of a granular GAC particle is shown in Fig. 1. More photographic material of examined GAC media is provided in the [Supplementary materials](#) (Section 1).

A Retsch (RT 6.5) sample splitter was used to obtain representative GAC samples for the reproducibility of the research analyses. Samples were washed to remove dust and fine particulate material, dried and stored for particle characterisation. GAC samples were then kept in water for six months before performing fluidisation experiments. Samples were periodically stirred to achieve the highest possible wetting degree of the internal pores. Locally produced drinking water was used in all experiments.

### 2.2. Porous media – dry and wet conditions

In the literature, the terms ‘voidage’ and ‘porosity’ are often used interchangeably. For this research, we use the term ‘voidage’

**Table 1**  
Examined GAC types.<sup>a</sup>

Grain material	Supplier	Source	Shape	$d_{10}$ <sup>c</sup>	$d_{50}$	$d_{90}$
Aquasorb K-6300	Jacobi	Fossil-based	Granular	0.77	1.15	3.10
Aquasorb K-6300 <sup>b</sup>	Jacobi	Fossil-based	Granular	n.a.	n.a.	n.a.
Aquasorb KGA	Jacobi	Green materials-based	Granular	0.67	1.07	2.62
Filtrisorb 300C	Calgon Chemviron	Fossil-based	Granular	0.66	0.90	2.24
Filtrisorb TL830	Calgon Chemviron	Fossil-based	Granular	0.99	1.31	2.77
Norit GAC 830 Supra	Cabot	Green materials-based	Granular	0.64	1.01	2.73
Norit RB 4C	Cabot	Green materials-based	Extruded	3.73	5.16	9.36
Norit ROW 0.8 Supra	Cabot	Green materials-based	Extruded	0.81	1.19	2.72
Resorb HC	Jacobi	Fossil-based	Granular	0.60	0.90	2.64
Saratech Spherical	Blücher Technologies	Polymer-based	Spherical	0.41	0.42	0.53

<sup>a</sup> Determined with a Camsizer [45].

<sup>b</sup> Long-term GAC from a full-scale filter with a retention time of approximately 2–3 years.

<sup>c</sup>  $d_{10,min}$  is the particle size for which 10% of the particles are smaller. Min refers to the width of the particles.



**Fig. 1.** Filtrisorb TL830 GAC.

in the same way as for rigid particles, defined as the fraction of the total volume, which is open space available for the fluid to flow around the particles; thus, the external porosity is similar to the voidage. The internal porosity is defined as the ratio of the internal pore volume to the whole nominal volume of a porous particle.

Unlike impermeable solid granular materials, porous GAC particles exhibit multiple densities and porosities based on different volumetric definitions [23,46,42,13]. Inclusion of closed and/or open pores and absorption of water can significantly influence the density [32]. For dry activated carbon, the mass and volume of pure coal without internal pores yields the absolute density  $\rho_a$ . The skeletal density  $\rho_s$  includes the closed pores as well. Including the (dry) open pores yields the particle (or envelope) density  $\rho_p$ . Taking the interparticle void space, or ‘external porosity’, into account yields the bulk density  $\rho_{bulk}$  which is usually the density provided by suppliers. A schematic overview is presented in Fig. 3. Prolonged submersion of GAC causes the open pores to absorb water, increasing the mass of the particles. The volume of water absorbed per mass of dry GAC is defined as the open pore volume or OPV, usually expressed in litres per gram. Complete filling of the open pores can usually only be achieved under vacuum [47]. As a vacuum is not applied in practice during the backwash of the investigated GAC particles, this is outside the scope of the current research. Therefore, in this research, open pores [48] were defined as the internal voids penetrated by water upon prolonged immersion for at least six months. The particles used in the experiments were wetted before and submerged during the fluidisation experiments. A main emphasis is therefore placed on the ‘wetted’

state of activated carbon. Three states of wetting can be defined: oven dry (OD), saturated surface dry (SSD) and wet surface (WS) conditions, as respectively shown in Fig. 2.

The saturated surface dry mass (SSD mass) is defined as the oven dry mass (OD mass) added to the mass of water inside the open pores, excluding water on the surface of the particles, as visualised in Fig. 2. In practice, a porous sample retrieved from immersion liquid is covered with a surface film that contributes non-negligibly to its mass [49]. This state is addressed as wet surface condition (WS condition), as seen in Fig. 2. The difficulty in differentiating between mass contribution of water on surface and water in pores complicates determining the SSD condition, which was emphasised most recently by Hunce et al. [13] and Cummins et al. [50]. To determine the SSD wet mass and wet density, information about the water permeable portion of the pores is required. Multiple experiments were used to acquire this information, ranging from immediate experiments to time-consuming experiments, the latter being eventually chosen to determine definitive values. According [51] and [32], a reproducible SSD condition is difficult to achieve and requires a certain level of experience and skill to perform.

For this research, a schematic overview of a single GAC particle was used, presented in Fig. 3, to distinguish external and internal parts of the particle. To differentiate the voids in the particle, open and closed pores are included as well as the rigid part, which is called absolute carbon. Closed pores are defined as pores that are inaccessible to water. The open pores can be partially or entirely filled with water to indicate the wetting state of a particle. All necessary equations are based on the schematic representation of a single GAC particle (Fig. 2) for OD, SSD and WS conditions, as discussed by Hunce et al. [32]. The model in Fig. 3 was used accordingly to derive the equations regarding bulk, particle, skeletal, wet density and open pore volume.

The relation between the bulk density  $\rho_{bulk}$ , (internally dry) particle density  $\rho_p$  and the external porosity  $\epsilon_{ext}$  (voidage) is given by van Keulen [52]; Sereno et al. [46]; Worch [42]; Hunce et al. [32]:

$$\epsilon_{ext} = 1 - \frac{\rho_{bulk}}{\rho_p} \tag{1}$$

Next, the wet density  $\rho_{wet}$  (open pores filled with water) can be calculated as a function of the particle density, water density  $\rho_w$  and the open pore volume OPV [42] as:

$$\rho_{wet} = \rho_p(\rho_w OPV + 1). \tag{2}$$

The wet density  $\rho_{wet}$  as a function of the OPV and skeletal density  $\rho_s$  was derived accordingly as Eq. (3).

$$\rho_{wet} = \rho_s \frac{1 + \rho_w OPV}{1 + \rho_s OPV} \tag{3}$$

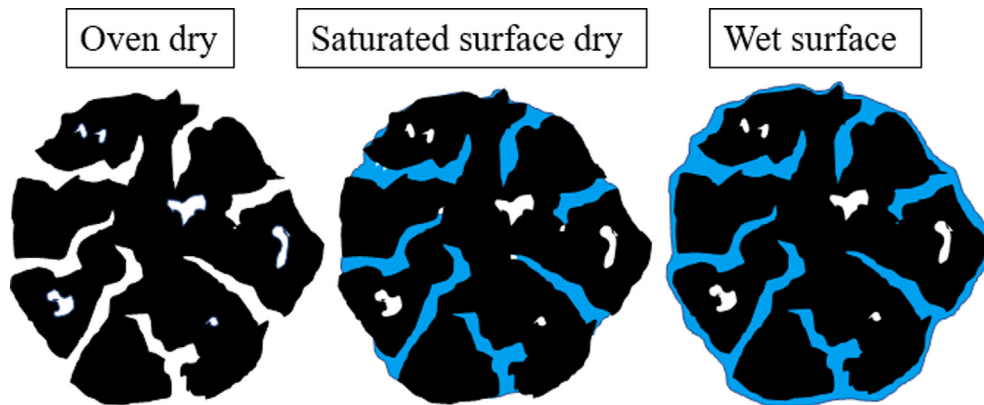


Fig. 2. Illustrations of oven dry, saturated surface dry and wet surface granular activated carbon pore structure [48].

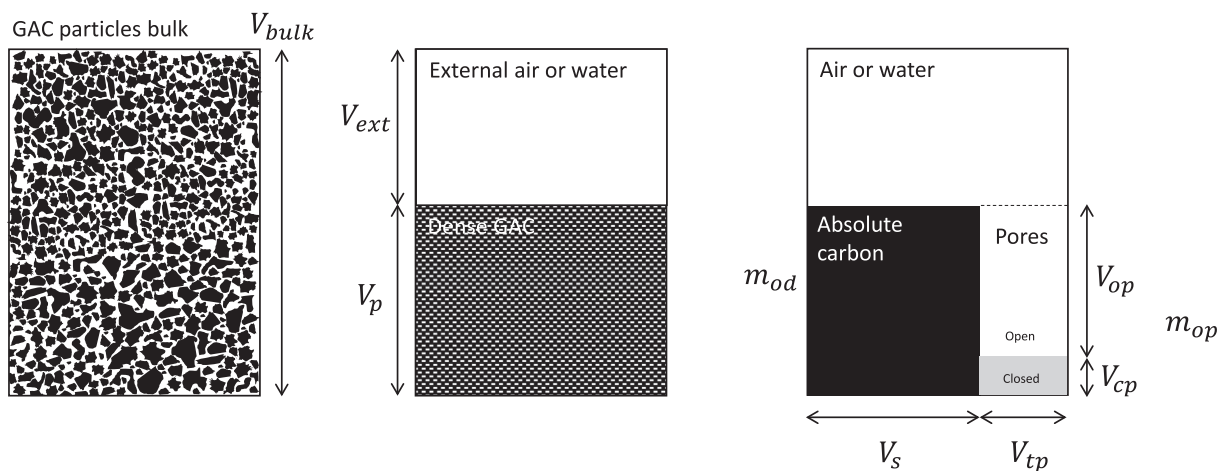


Fig. 3. Schematic model representation of a GAC particle.  $V_{bulk}$  is the bulk volume or GAC particles including external voids,  $V_{ext}$  is the external volume of the external voids,  $V_p$  is particle volume including internal pores,  $m_{od}$  is the oven dry particle mass,  $V_{op}$  and  $m_{op}$  are the open pore volume and mass,  $V_{cp}$  the close por volume,  $m_{cp}$  represents the open pore mass which can by dry or wet,  $V_s$  is the skeletal volume and  $V_{tp}$  is the total pore volume.

Detailed information about GAC modelling, nomenclature and derivations can be found in the [Supplementary materials](#) (Section 7).

### 2.3. Laboratory measurements – particle characterisation

#### 2.3.1. Particle size and shape determination

A number of methods were used to define the size and morphology of particles. First, *classical sieving*, a frequently applied method, was used to physically separate particles using a mesh. Particles smaller than the mesh size can pass through to the next mesh and larger particles will be retained in the mesh. Second, static image analysis was used, where a referenced picture or scan of a GAC sample was analysed using specialised software such as ImageJ [53] to analyse pixels and a microscope with internal software [54]. The software computes the size and different morph parameters of each particle in the picture. This method generates different dimensions of irregularly shaped particles and many other morphological parameters. Third, dynamic Camsizer image analysis was used [45] to analyse a large number of falling particles with high-speed cameras coupled with specialised software. Detailed information about particle characterisation, applied methods and morphological properties of examined GAC media is provided in the [Supplementary materials](#) (Section 2). Experimentally obtained data is also shared in [55].

#### 2.3.2. Particle density and wetting degree determination

##### Oven dry mass and bulk density

The GAC samples were dried in an oven at 150 °C for two days, to guarantee optimal drying and at the same time prevent possible loss of material due to the heating. The weight  $m_{od}$  was measured on scale (type Kern FKB). The bulk density  $\rho_{bulk}$  was determined according to Eq. (4) by measuring the bulk volume in a graduated cylinder [39].

$$\rho_{bulk} = \frac{m_{od}}{V_{bulk}} \quad (4)$$

Note that the bulk volume  $V_{bulk}$  and thus the external porosity is dependent on the arrangement of the particles. Variations can be observed once the bulk collapses when vibrations are applied and when particles are stratified, such as during the expansion experiments.

##### Skeletal density

Two methods were employed to determine the skeletal density. *Helium pycnometry*

First, helium pycnometry (type using an AccuPyc 1330) [56,57] was applied. Helium was added under pressure in the specialised apparatus, entering all accessible pores in a dry GAC sample. Based on the pressure increase and added helium, the helium impenetrable volume was determined which, combined with the dry mass of the sample, yields the skeletal density  $\rho_s = m_{od}/V_s$ . More detailed information is elucidated by Sereno (2007) [46].

### Hydrostatic weighing

Subsequently, hydrostatic weighing took place. This is an established technique for density determination [52,49] which applies the *Archimedes* principle [58] to determine the volume of a sample by measuring the weight loss upon submersion caused by the buoyant force. The skeletal or ‘in-accessible by water’ density was determined using:

$$\rho_s = \frac{\rho_w}{1 - \frac{m_{sub}}{m_{od}}} \quad (5)$$

where  $m_{od}$  is the oven dry mass and  $m_{sub}$  the submerged SSD particle mass.

Detailed information about the helium pycnometry and hydrostatic weighing techniques can be found in the [Supplementary materials](#) (Section 3) and in [59] and [55].

### Wet density and SSD mass

Three methods were employed to determine the water penetrable portion of the activated carbon samples.

#### Wet bulk

Wet bulk GAC samples were placed in a calibrated graduated cylinder. Water was removed until slightly above the sample and excess water was removed with a paper towel. Any air pockets were removed. The measured total particle volume in the graduated cylindrical column is indicated by  $V_{bulk}$ . The mixture was weighed  $m_{meas}$ , and the SSD mass of the GAC sample was defined as:

$$m_{ssd} = m_{meas} - \rho_w(V_w - V_{bulk}(1 - \epsilon_{ext})) \quad (6)$$

To find  $m_{ssd}$ , the external porosity  $\epsilon_{ext}$  obtained from the fluidisation experiments (Sections 2.4 and 3.3) was used.

#### Drained sieve

The wet samples were placed on a sieve and drained; excess water was wiped away with a paper towel until the samples appeared visually dry. This technique is commonly used [56,60,32] but the inability to determine exactly when SSD conditions are reached makes the results of this method rudimentary at best. The tendency to retain water on the surface differs between carbon types, and it was estimated that excess water was still present even after repeatedly wiping away the water, especially for the smaller grains such as Saratech Spherical and Norit ROW 0.8 Supra.

#### Drying log

To identify the SSD condition, or rather the more explicit (Eq. (7)), a total of 42 drying logs were measured. Representative samples of 5–25 [g] of each GAC-type were administered in wet surface condition (Fig. 2) in a thin layer on a non-absorbent surface. The weight of these samples was measured on a scale connected to a data logger for three to six days at room temperature in a closed fume hood with no ventilation. Initially, a linear, constant drying rate was expected, characterised by an excess of liquid in the surface pores of the porous particles [61]. The weight decrease during this period is assumed to be predominantly caused by the evaporation of the adhesion layer (water on the surface) [49]. The initial drying rate was expected to decrease significantly, or drop to zero, when surface dry conditions are met [62]. During this period, drying is controlled by mass transport mechanisms within the porous material [63], which will not be discussed in this research. SSD mass, or  $m_{ssd}$ , was identified by extrapolating the last part of the drying log to  $t = 0$ , as seen in Section 3, Fig. 5. The water content at any point of the measurement could be determined after the oven dried mass  $m_{od}$  was acquired by placing the partially dried samples in an oven at 100 °C until the change in weight was negligible ( $\approx 8$  h). This resulted in Eq. (7) for the OPV and Eq. (3) for the wet density:

$$OPV = \frac{\frac{m_{ssd}}{m_{od}} - 1}{\rho_w} \quad (7)$$

More detailed information and visual displays concerning the drying log method can be found in the [Supplementary materials](#) (Section 3).

### Particle density

The particle density was determined indirectly by using the open pore volume and the skeletal density using the following:

#### Mass balance equation

Based on the GAC model (Fig. 3), the particle density can be calculated when the OPV and skeleton density are known:

$$\rho_p = \frac{1}{\frac{1}{\rho_s} + OPV} \quad (8)$$

#### Image analysis

The particle envelope density could also be determined using the embedded image analysis software in a VHX microscope. This workflow consisted of obtaining a 3D model of the particles with the image processing software. This model helped determine the average height of several particles in the sample. After the average height of particles is determined, the area can also be easily calculated to obtain the volume of the particles in the sample. When this envelope volume is known, it suffices to know the mass of the analysed particles to determine the particle density. Detailed information about the particle density determination and GAC modelling can be found in the [Supplementary materials](#) (Sections 3 and 7).

## 2.4. Fluidisation measurements – expansion characteristics

Expansion experiments for GAC grains were carried out at three locations: in Waternet’s Weesperkarspel drinking water pilot plant located in Amsterdam, the Netherlands; at the University of Applied Sciences Utrecht, the Netherlands; and at Queen Mary University of London, United Kingdom. In the experiments, locally produced drinking water was used. The set-up (Fig. 4) consisted of a 4-meter transparent PVC pipe with an inner diameter of 57 mm. Water temperature was regulated with a boiler, a cooler and a thermostat by recirculating water through a buffer vessel connected to a water reservoir. An overflow at the top of the reactor returned water to the buffer vessel. From the buffer vessel, water was pumped through the reservoir connected to the thermostat which was set to a programmed water temperature. A frequency modulated gear pump was used to enable a fluidisation velocity range suitable for the selected samples and prevent flow fluctuation. Differential pressure, superficial velocity, bed height and temperature were measured for 20–40 velocities, corresponding to a total of 53 fluidisation experiments for calibration and 30 for validation purposes. Water temperatures ranged from 4 to 40 °C. The velocity and temperature ranges were selected to cover the temperatures and velocities that are applied for the backwash procedure at Waternet throughout the year (5 to 20 °C).

Detailed information about expansion experiments, technical details about used equipment, standard operational procedures, photographic material, videos and applied methods is included in the [Supplementary materials](#) (Sections 1, 4, 5 and 10). Experimentally obtained expansion data is shared at [55].

## 2.5. Modelling aspects – voidage and incipient fluidisation

To predict the fluidisation behaviour, *i.e.* voidage (external porosity), of GAC, several important input parameters are required for the modelling exercise. The inputs consist of several particle

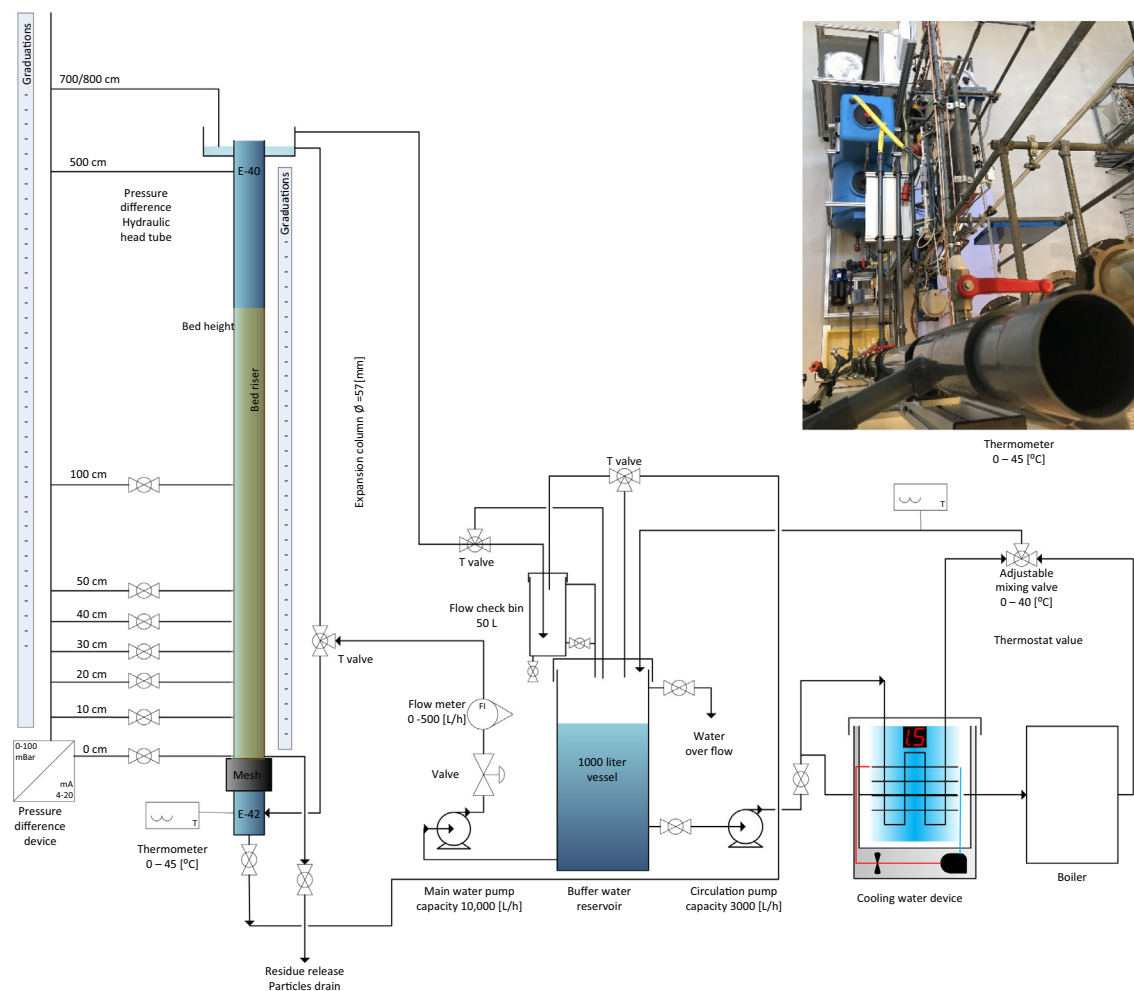


**Fig. 4.** Schematic representation of the experimental set-up. The expansion columns have two main circuits in which water flows: the expansion circuit and the temperature conditioning circuit. In the expansion circuit, a pump takes water from a reservoir and feeds it to the expansion column with an adjustable water flow. The flow rate entering the system can be controlled by opening and closing a valve in combination with an installed flow meter. The pressure drop was measured with a differential pressure sensor. The temperature conditioning circuit was used to deliver a desired temperature to the expansion circuit to perform expansion experiments at different temperatures. The circuit consists of a pump that feeds water into an integrated heating or cooling unit. Granular activated carbon particles are fluidised in a cylindrical transparent tube.

characteristics (size, density, morphological properties), which were determined using various methods. For solid spherical monodisperse particles, the voidage can be predicted accurately as a function of fluid properties (velocity and viscosity) and particle properties (size and density) [64–67]. For non-spherical, polydisperse and porous GAC particles, the voidage prediction is considerably more complex. For the sake of convenience, the spherical particle size is commonly used in prediction models. Few models use morphological particle properties. Ergun [21], however, included the particle shape factor. In the scientific literature, substantial knowledge is available regarding particle morphology: [68–71,64,72–77]. One of the most frequently used morphological properties is the sphericity proposed by Wadell [78]. However, in fixed beds, shape factors are more commonly used to match the predicted with experimentally obtained voidages [40], or they are omitted. Voidage prediction models are only valid for a fluidised state. For this reason, it is important to determine the incipient fluidisation point to check the prevailing state. The onset of fluidisation from fixed to fluidised state occurs when the drag force is equal to the weight of the particles. Although numerous prediction models are proposed in the literature, such as [79,21,80,64,81] there is no general agreement about the best approach. The degree of irregularity and polydispersity of particles as well as influences

caused by the packing factor, surface forces and wall effects increase the complexity of accurate prediction.

The focus in this research lay on gaining insight into fluidisation characteristics and to a lesser extent on proposing accurate voidage prediction models. Nevertheless, the experimentally obtained expansion characteristics were compared to the most popular voidage prediction models proposed by Carman [20]; Ergun [21] and Richardson and Zaki [22]. Accordingly, a data-driven model was used to predict the effective voidage proposed by Kramer et al. [66] based on dimensionless numbers (Rep1Frp model). In addition, a model based on symbolic regression was considered [82]. Minimum fluidisation prediction, fluidisation modelling details and graphs are given in the [Supplementary materials](#) (Section 6).

### 3. Results and discussion

#### 3.1. Porous media – dry and wet conditions

Wetted GAC grains were analysed to obtain the open pore volume and wet density via the wet sieve method and drying log curve method. The results are presented in Fig. 6. For most of the eight GAC types, the OPV values provided by manufacturers (or-

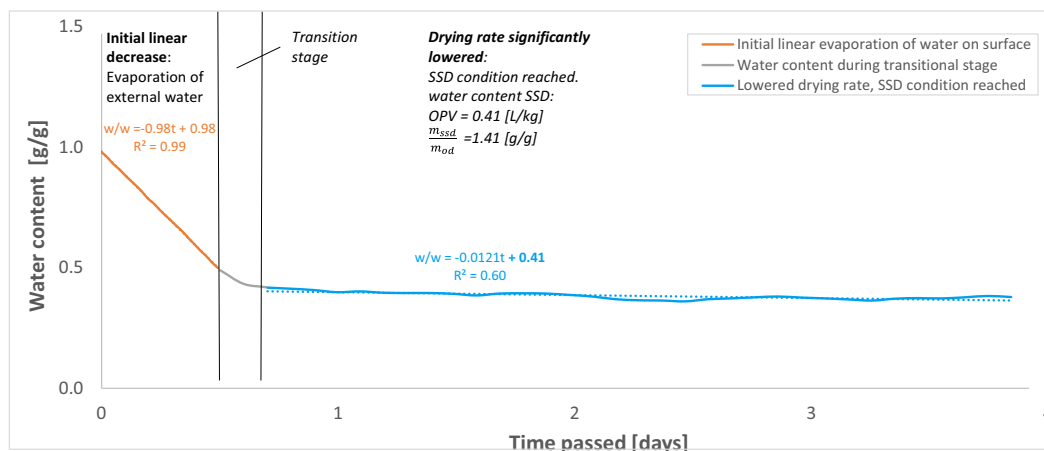


**Fig. 5.** A typical drying log curve for Norit GAC 830 Supra. There are three stages: initial linear decrease with fast evaporation of external water, a transition stage and the saturated surface dry condition in equilibrium with the environment.

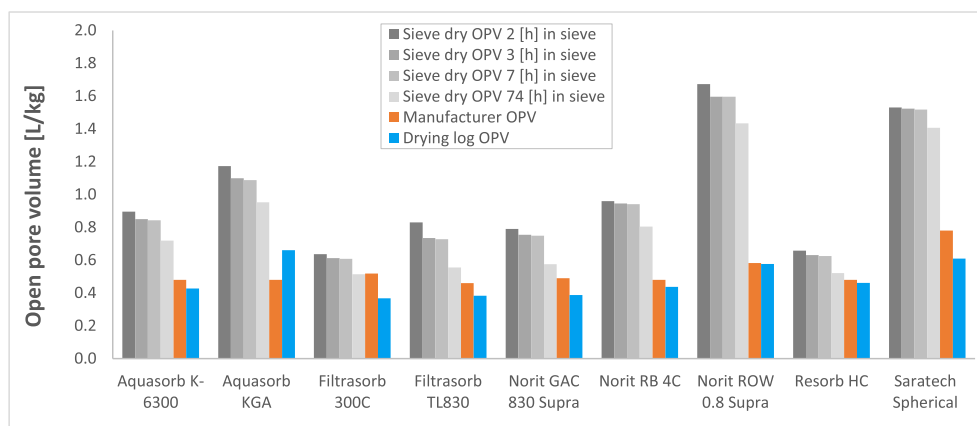


**Fig. 6.** Open pore volumes, experimentally determined and provided by the suppliers.

ange bars) were slightly higher ( $\approx 14\%$ ) than our experimentally determined drying log values (blue bars). The more commonly used sieve drying method [32] values (grey bars) are considerably higher ( $\approx 77\%$ ), even with longer drying times.

### 3.1.1. Drying log

In the drying logs (example in Fig. 5), we observe an initial linear decrease due to evaporation of external water. While it is possible that water from the largest pores might be transported to the surface through capillary forces during the initial constant rate period, the drying logs do in fact consistently show a sharp decrease of drying rate after a certain time depending on the GAC type used. The variations of the 42 measurements, caused a standard deviation of  $\approx 7\%$  for the open pore volume, with a maximum of 20% for Aquasorb K-6300. The effect of the deviation or data spread in OPV on the error of the wet density was  $\approx 1\%$  using Eq. (3). An example of a drying log graph is shown in Fig. 5. The drying methodology can be improved by using conditioned lab circumstances (taking the temperature and relative humidity into account) to increase the validity of this approach.

A large data set consisting of more than one million individual drying log measured data points is shared in [55], and additional methodology information about methylene blue adsorption can be found in the Supplementary materials (Section 3).

### 3.1.2. Wet sieve

Draining and wiping excess liquid seemed to remove the external bulk water only partially, as the wet mass found using this technique was substantially higher than the wet mass found using the other two techniques. Similar results were found by Hunce et al. [32], who used a similar approach. Especially for the smaller particles such as Saratech Spherical and Norit ROW 0.8 Supra, in which water could not escape as easily, an increased mass was found.

## 3.2. Laboratory measurements – particle characterisation

### 3.2.1. Particle size and shape determination

Four methods were employed to determine the particle size of each sample, starting with the classical sieve analysis, microscope static image analysis, ImageJ static image analysis and accordingly a Camsizer dynamic image analysis, represented in Table 2. All other particle size and morphological GAC properties determined are provided in the Supplementary materials (Section 2).

Regarding spherical GAC particles, such as Saratech, the  $d_{10}$  for all four methods was, as expected, more or less the same  $0.42 \pm 0.02$  mm. The granular GAC grains gave different results for the applied methods. Compared to the sieve analysis, the microscope  $d_{10}$  was approximately  $\approx 15\%$  smaller but with a con-

**Table 2**  
Sieve analysis, microscope, ImageJ and Camsizer effective sizes.<sup>1)</sup>

Shape	GAC type Note Variable Unit	Sieve		Microscope		ImageJ		Camsizer	
		$d_{10,SP}$	$d_{50,SP}$	min	max	min	max	min	max
		[mm]	[mm]	$d_{10,min,MIC}$	$d_{10,max,MIC}$	$d_{10,min,IJ}$	$d_{10,max,IJ}$	$d_{10,min,CS}$	$d_{10,max,CS}$
Granular	Aquasorb K-6300	1.27	1.67	1.33	1.96	1.41	2.02	0.77	1.15
Granular	Aquasorb KGA	0.89	1.38	0.95	1.41	1.08	1.42	0.67	1.07
Granular	Filtrisorb 300C	0.93	1.51	0.75	1.03	1.08	1.42	0.66	0.90
Granular	Filtrisorb TL830	1.27	1.56	0.86	1.26	1.35	1.92	0.99	1.31
Granular	Norit GAC 830 Supra	1.07	1.64	0.97	1.45	0.95	1.45	0.64	1.01
Granular	Norit RB 4C	3.15	4.55	3.79	6.05	4.05	5.29	3.73	5.16
Extruded	Norit ROW 0.8 Supra	0.81	0.86	0.82	1.64	0.85	1.57	0.81	1.19
Extruded	Resorb HC	0.94	1.48	0.84	1.22	1.26	1.82	0.60	0.90
Granular	Saratech Spherical	0.43	0.47	0.41	0.44	0.39	0.42	0.41	0.42

<sup>1)</sup>  $d_{10,min}$  of minimum diameter (minor axis of ellipse) and  $d_{10,max}$  of maximum diameter (major axis of ellipse).

siderable standard deviation ( $\approx 15\%$ ), possibly due to the fact that only a few grains were analysed compared to ImageJ where 10 or 100 times more grains were analysed per run. ImageJ measurements were approximately  $\approx 10\%$  larger compared to the sieve analysis (with a slightly lower standard deviation  $\approx 10\%$ ) due to the particle orientation. Elongated particles pass the sieve in a vertical orientation in contrast to the horizontally oriented grains on the scanner. The Camsizer measured considerably lower ( $\approx 30\%$ )  $d_{10}$  values compared with the sieve results. The  $d_{10,max,CS}$  instead of the  $d_{10,min,CS}$  agreed reasonably well with the  $d_{10,SP}$ .

GAC grains in general have a wide particle size distribution PSD. When these mixtures with a large PSD, i.e. with a wide range in particle sizes, are fluidised, the smallest particles have the tendency to expand the most. For that straightforward reason, the  $d_{10}$  (the particle size which corresponds to 10 percent finer on the cumulative PSD curve) or effective size is often used [13] to represent the input variable  $d_p$  in hydraulic models. The sieve analysis only provides 1D information. The microscope reveals more 3D information about GAC, but only a small number of grains can be investigated. The Camsizer analysis covers a larger number of grains, but the particle orientation is less clear compared with the ImageJ method. This latter method is more cost effective and a sufficient number of grains can be analysed, which is imperative when samples with a wide PSD are concerned. Detailed information about particle characterisation, applied methods and morphological properties of examined GAC media are provided in the Supplementary materials (Section 2). Experimentally obtained data is shared at [55].

### 3.2.2. Density determination

The bulk, skeletal, particle and wet density (Eqs. (4), (5), (8) and (3)) were determined for the nine GAC types. The results are

presented in Fig. 7. The absolute density of activated carbon [83] and water were added as a reference for comparison.

The error for the bulk density (orange bars) determined with the gradient cylinder compared with the manufacturer's value was  $\approx 7\%$  and is in agreement with Chowdhury et al. [12]. The determined dry particle density (grey bars) fluctuated around the water density observed visually as some dry GAC particles floated and some slowly settled to the bottom of the jar. The skeletal density (dark grey bars) for all GACs was lower than the absolute density of activated carbon [83,7,9]. The most relevant density for this research is the wet density (blue bars), which is used in the hydraulic models. For all nine GAC types, the average wet density was  $1,450 \pm 50$  ( $\approx 4\%$ ). Graphical results of densities, porosities and particle mass for each GAC type can be found in the Supplementary materials (Section 3). The wet density was also determined with the differential pressure sensor of the expansion experimental set-up for validation purposes (Section 3.3).

### 3.2.3. Voidage determination

The voidage of non-stratified GAC (Fig. 8) was determined with a graduated cylinder/pycnometer and with Eq. (1) based on the particle density and bulk density or wet density (blue bars). The voidage of stratified GAC was also determined using the fixed bed in the expansion experiments (Section 3.3). The voidage at minimum fluidisation conditions is, as expected, slightly higher than the (stratified) fixed bed voidage but considerably higher than the non-stratified values. This is caused by the large PSD where smaller grains can fill the voids between the larger grains, thus decreasing the voidage. The common fixed bed voidage for rigid spherical particles was added in Fig. 8 as a reference. The voidage for granular GAC was found to be  $0.57 \pm 0.05$ , considerably higher than some values obtained from the literature (Section 1), which is in line with the water standard works by Crittenden et al. [2]

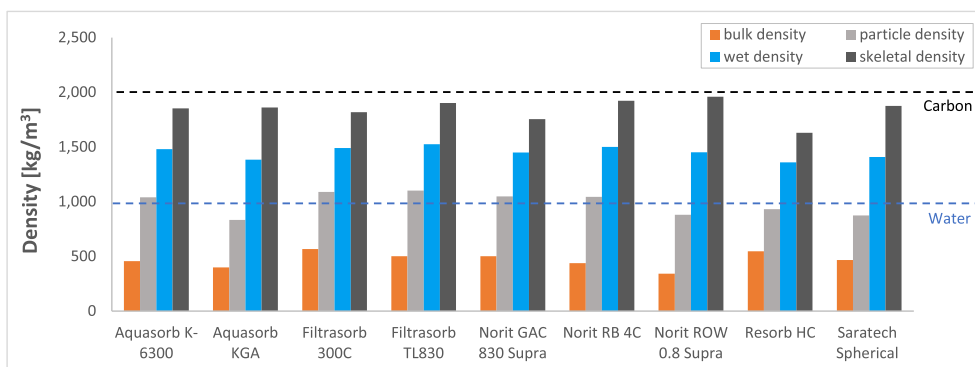


**Fig. 7.** Experimentally determined densities. The absolute density of activated carbon [83] and water were added as a reference [84].

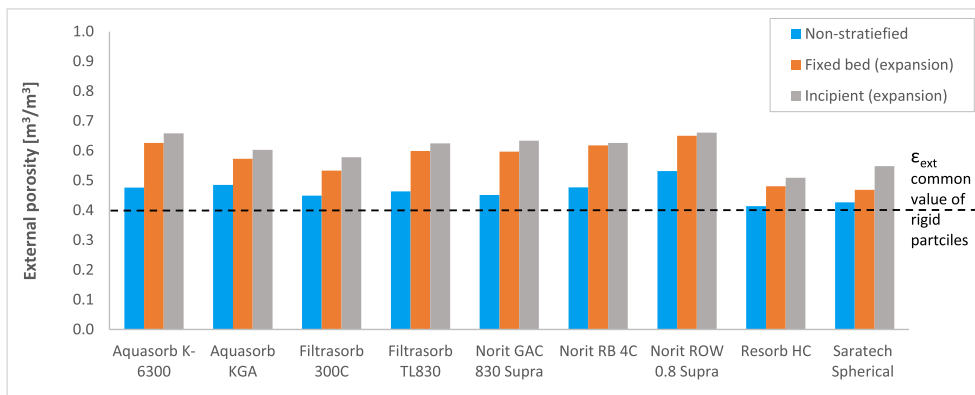


Fig. 8. Experimentally determined voidage (external porosities). The commonly used fixed bed porosity for rigid spherical particles was added as a reference [64].

and by van Lier [23]. Rod-like GAC had a slightly higher voidage  $0.63 \pm 0.02$ , which is most likely caused by the elongated particle shape and degree of packing. Spherical GAC, in contrast, had a voidage of 0.47, which is lower than the other GAC types. The values determined by the expansion experiments (Section 3.3) were as follows: granular:  $0.60 \pm 0.05$ , rod-like:  $0.64 \pm 0.02$  and spherical 0.55, respectively.

### 3.3. Fluidisation measurements – expansion characteristics

A total of 48 liquid-solid fluidisation experiments were carried out to gain insight into the expansion characteristics of GAC grains. The obtained data was used to compare the experimentally

obtained voidage with the prediction models. In addition, some models were calibrated with these expansion data. Thirty fluidisation experiments were used for model validation purposes. Five additional experiments were performed with long-term GAC obtained from a full-scale GAC filter. Fig. 9 shows typical expansion curves for voidage (external porosity) and differential pressure as a function of superficial fluid velocity for temperatures between 4 °C and 31 °C.

The experimental dataset acquired consisted of a matrix with varying temperatures, grain sizes and flow rates.

In the fixed bed state, the voidage is  $\approx 0.6$  (Table 3), which increases in the fluidised state for further elevated superficial fluid flows. The temperature (viscosity) effect is clearly visible and fol-

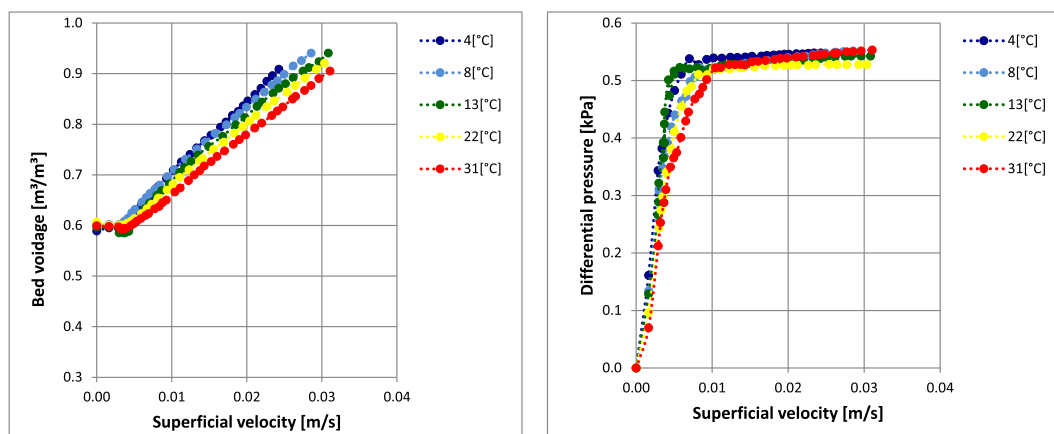


Fig. 9. Experimental expansion characteristics of Norit GAC 830 Supra.

Table 3

Experimentally determined and estimated fixed bed and incipient fluidisation voidages and average relative errors for individual GAC types.

Grain material	Shape	$\epsilon_0$	$\epsilon_{mf}$	$\epsilon_{mf,CK}$	ARE
Aquasorb K-6300	Rocks	0.63	0.66	0.45	–31%
Aquasorb K-6300 <sup>1)</sup>	Rocks	0.62	0.65	0.54	–18%
Aquasorb KGA	Rocks	0.57	0.60	0.50	–18%
Filtrasorb 300C	Rocks	0.53	0.58	0.50	–13%
Filtrasorb TL830	Rocks	0.60	0.62	0.47	–24%
Norit GAC 830 Supra	Rods	0.60	0.63	0.54	–15%
Norit RB 4C	Rods	0.62	0.63	0.38	–40%
Norit ROW 0.8 Supra	Rocks	0.65	0.66	0.42	–36%
Resorb HC	Rocks	0.48	0.51	0.47	–7%
Saratech Spherical	Balls	0.47	0.55	0.69	27%

<sup>1)</sup> Long-term GAC from a full-scale filter with a retention time of approximately 2–3 years.

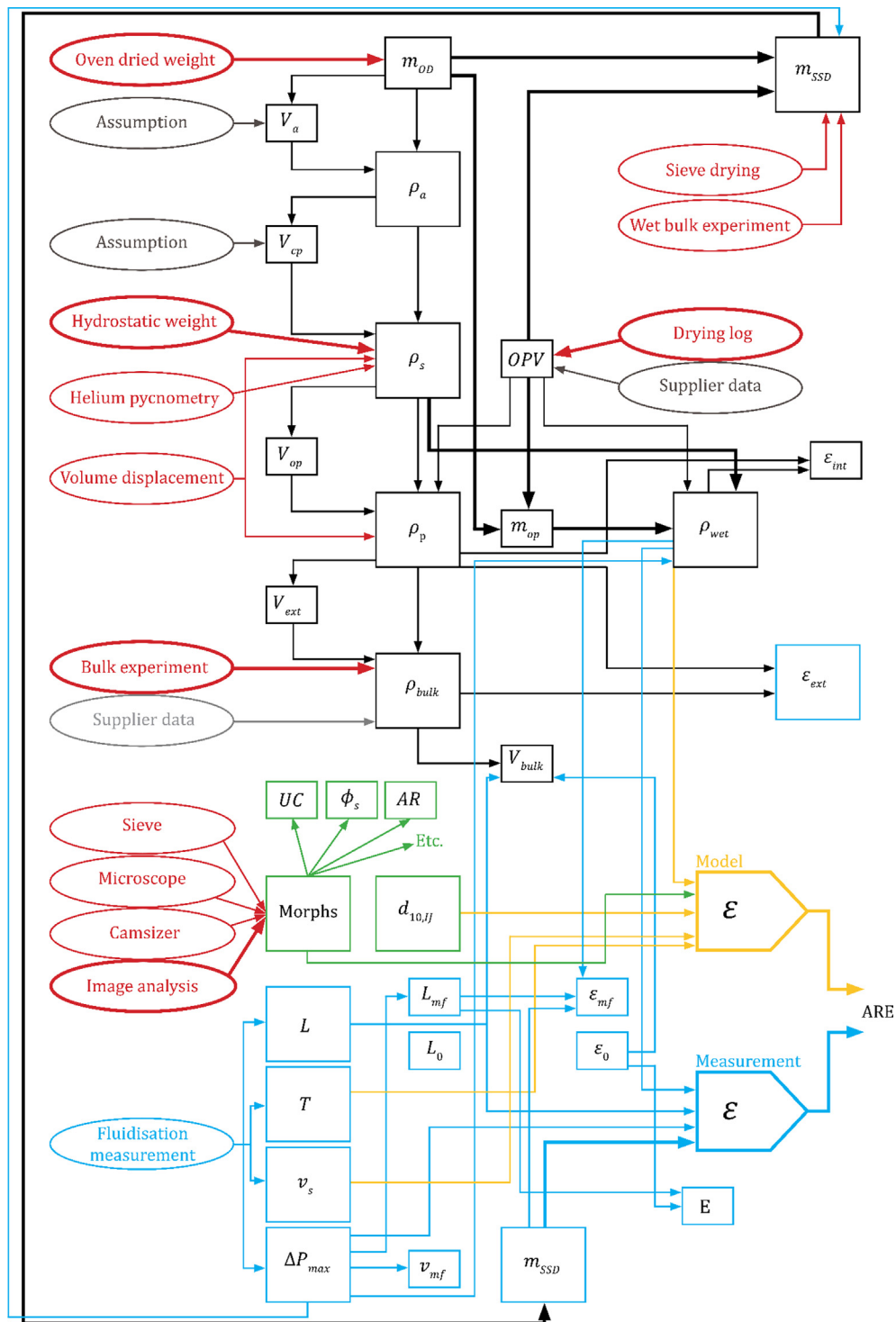


Fig. 10. GAC conundrum scheme. Bold lines indicate the route followed in this work. For the meaning of colours, we refer to the main text.

lows the same characteristics compared to rigid particles. The only difference is the incipient fluidisation point, which is significantly larger ( $\approx 0.6$ ) compared to spherical particles ( $\approx 0.4$ ) [64,85,65]. The differential pressure shows a transition trajectory from fixed to fully fluidised state. Due to the large PSD, the smallest grains ( $\approx 0.64$  mm) start to fluidise in an earlier state compared to the larger grains ( $\approx 2.73$  mm). This confirms the complexity regarding the prediction of the incipient fluidisation of polydisperse GAC. Expansion curves for all GAC types are provided in the [Supplementary materials](#) (Section 5).

### 3.4. Modelling aspects – voidage, morphology and incipient fluidisation

In the scientific literature, many models have been proposed to estimate the minimum fluidisation velocity as a function of the particle properties. The Wen–Yu model [79] is one of the most commonly used models. The average relative error between the predicted and measured minimum fluidisation velocity model was  $\approx 38\%$  for granular grains,  $\approx 14\%$  for rod-like grains and a considerable  $\approx 78\%$  for spherical particles. In fact, the minimum fluidi-

sation velocity is relevant for effective backwashing but can hardly be predicted accurately. Applying discretisation modelling, *i.e.* dividing the bed in separate layers with a distinct particle diameter related to this particular layer, could provide a solution for the particle size as input parameter in the prediction model. This approach does not, however, solve the other mentioned GAC-related challenges.

The well-known Carman–Kozeny model was used to estimate the incipient voidage under minimum fluidisation conditions. Table 3 presents the accurately measured fixed and incipient voidages as well as the estimated incipient voidage as determined with the Carman–Kozeny model. The average relative error between the predicted and measured incipient voidage was  $\approx 19\%$  for granular grains,  $\approx 38\%$  for rod-like grains and  $\approx 27\%$  for spherical particles. Although the Carman–Kozeny model is a well-established and often used model for solid and relatively spherical particles, it is less suitable for GAC grains. More detailed information is given in the Supplementary materials (Section 6).

The prediction of the voidage of GAC is complex as the particles are non-spherical, porous and polydisperse. Varying raw materials, manufacturing processes and pore structures further complicate the characterisation of the particles. Particularly the wet density, wet mass and the point of incipient fluidisation are difficult to determine. To be able to predict the voidage, these values must be known. In the literature, there is no general agreement regarding effective bed-voidage model prediction and employed spherical particles.

In this work, we combined advanced particle laboratory experiments and accurate liquid-solid fluidisation experiments. This led to the input parameters for the voidage prediction model. A schematic flowchart is given in Fig. 10. The GAC scheme consists of ovals (dark red) representing laboratory experiments. Squares (black) indicate the particle properties that are needed in the whole system. Input data from suppliers and assumed values are coloured grey. Green stands for morphological particle properties. The squares in blue represent hydraulic fluidisation experiment data. Yellow arrows are the input values for the model that leads to a voidage prediction. Finally, the prediction error can be calculated based on the model output and measured voidage. The GAC scheme in Fig. 10 shows the relationship between all the variables. Multiple routes are possible. We decided to choose the route with, at least to our knowledge, the highest reproducibility and transparency. This route is indicated by bold arrows.

The starting point of the solution to the GAC conundrum, shown in Fig. 11, is the SSD GAC particle (Fig. 2). The oven dry particle mass  $m_{od}$  can be measured directly. The skeletal density  $\rho_s$  was determined using the hydrostatic weighing technique (Eq. (5)) and accordingly the open pore volume using Eq. (7). From the SSD conditions, the wet particle mass  $m_{ssd}$  and wet density  $\rho_{wet}$  can be calculated (Eq. (3)). Regarding the particle size and shape, we chose the  $d_{10}$ . Various modelling results using symbolic regression can be found in the Supplementary materials (Section 6). Voidage prediction including morphological properties and symbolic regression including morphological properties, however, were not the focus of this work. By using morphological properties such as ellipsoid sizes, the particle orientation could be taken into account for a more accurate understanding of fluidisation behaviour and characteristics. With the fluidisation experiments, the differential pressure  $\Delta P_{max}$  could be used to validate the wet density  $\rho_{wet}$  or the SSD particle mass during fluidised bed state conditions (Eq. (9)):

$$\rho_{wet} = \frac{\rho_f}{1 - \frac{\Delta P_{max}}{m_{ssd}g} \frac{\pi}{4} D^2} \quad (9)$$

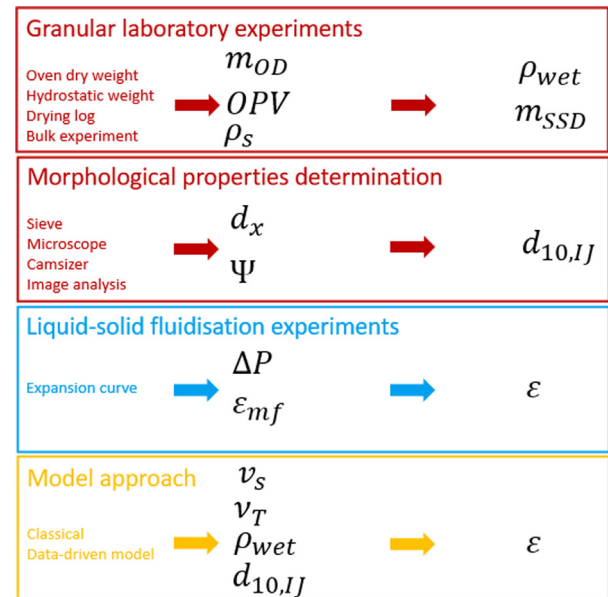


Fig. 11. GAC conundrum solution scheme.

*Vice versa*, the differential pressure or the external porosity could be checked with:

$$\frac{\Delta P_{max}}{L} = (\rho_{wet} - \rho_f)g(1 - \epsilon_{ext}) \quad (\epsilon > \epsilon_{mf}) \quad (10)$$

The differential pressure gauge is a sensitive and rather accurate measurement device, but it only works well if the occurrence of trapped air is prevented. Especially for grains with a small particle-to-fluid density ratio  $\rho_{wet}/\rho_w$  such as GAC, an initial non-zero off-set adversely affects the accuracy of  $\Delta P_{max}$  or  $\epsilon_{ext}$ . Initial off-set ranging from 0.75–3.25 mbar was found, which was accounted for by subtracting the  $\Delta P_{max}$  with the initial off-set. For this reason, the differential pressure was only used for validation purposes.

The fluidisation experiments could be used to determine the incipient voidage (Fig. 8) reasonably well, using the differential pressure transition from an increasing to a constant value. Based on the bed height, SSD mass and the wet density  $\rho_{wet}$ , the voidage of the system could be calculated. The SSD mass and wet density are crucial model variables. Their validity is not ensured entirely but may be improved upon improving the reliability of the GAC conundrum scheme. Graphical results of densities, porosities and particle mass can be found in the Supplementary materials (Section 3).

The SSD particle mass  $m_{ssd}$  together with the wet density  $\rho_{wet}$  combined with the fluid properties (superficial fluid velocity and viscosity) and the ImageJ  $d_{10,IJ}$  enabled average voidage prediction of the GAC beds. The most common hydraulic models were used to compare the estimated and experimental voidages. The voidages found experimentally were significantly higher compared to the classical predicted voidages estimated with the classical models. Finding fitting parameters for each of these models is fairly straightforward, but the usefulness of applying these fitted models is questionable (see Table 4).

The classical sieve analysis is still often used but provides only one-dimensional information about particles. It is also cumbersome. When the models must be improved, the sieve analysis is the least suitable method for further exploration. Other methods such as ImageJ analysis might be more suitable. The  $d_{10}$  can be

**Table 4**  
Voidage (external porosity) model prediction accuracy.<sup>1)</sup>

Model	Reference	MAE	ARE	NRMSE	LRMSE	R <sup>2</sup>
Carman–Kozeny	[20]	0.1279	16.8%	17.3%	19.6%	0.99
Ergun	[21]	0.1431	16.5%	19.5%	22.4%	0.99
Richardson–Zaki	[22]	0.2012	26.5%	26.7%	32.1%	0.99
Rep1Frp (fitted)	[66]	0.0337	4.5%	5.0%	5.0%	0.99

<sup>1)</sup> Mean average error (MAE), Average relative error (ARE), Normalised root mean square error (NRMSE), Logarithmic root mean squared error (LRMSE), correlation coefficient (R<sup>2</sup>).

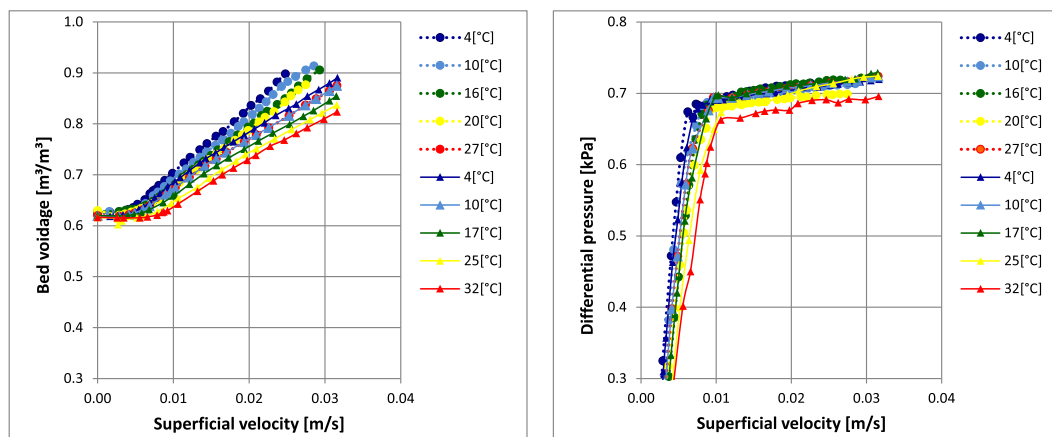


**Fig. 12.** Experimental expansion behaviour of Aquasorb K-6300 virgin GAC (circles) and long-term Aquasorb K-6300 GAC (squares) from a full-scale filter with a retention time of approximately 2–3 years.

used as an input parameter to deal with a large PSD. Discretisation modelling for GAC types with a large PSD could provide a more suitable solution.

Besides being non-spherical, GAC grains are polydisperse, porous and sensitive to attrition due to abrasive circumstances during backwashing and transport [86,87,83,18,77,17]. In addition, in full-scale filters, a biofilm layer may grow on GAC grains, affecting the drag and consequently the behaviour of the particles during fluidisation. Therefore, we compared one GAC type on its expansion characteristics. Aquasorb K-6300 virgin and Aquasorb K-6300 with a long-term retention of approximately three years in a full-scale drinking water filter were compared (Fig. 12). The expansion degree of the virgin GAC was approximately 10% larger compared to the bio GAC. This is most likely caused by the reduction of fines which were flushed out of the system, a slightly increased density caused by intake of OMPs and the growing biofilm. The graphs can be found in the [Supplementary materials](#) (Section 5).

#### 4. Conclusions

##### – Scientific conclusions

In this research we developed a new approach leading to new insight into the expansion characteristics of granular activated carbon grains used in water fluidisation processes. The scientific literature is not in agreement about how - and especially how accurately - the fluidisation characteristics of granular activated carbon (GAC) grains can be predicted. Some researchers propose empirical models and mention low prediction errors, but it is unclear how accurate these models will remain when GAC is used for a long period of time. We demonstrated that it is possible to combine GAC particle laboratory experiments with hydraulic experiments and mass balance-based equations. The incipient voidage, the saturated surface dry mass and wet density can be derived from both fluidisation and laboratory experiments. Conse-

quently, it is possible to improve the validity of the variables which can be used to predict the voidage more accurately.

##### – Effect on design

In this work, we showed that fluidisation behaviour of GAC is very complex due to polydispersity, its porous character and non-spherical properties of the grains. Therefore, traditionally, full-scale GAC filters are commonly over-designed to cope with fluctuations and variations. For reliable and safe drinking water production however, a precise specification of backwash rates for filter cleaning is needed to prevent mudball, short circuiting and fixed bed formation, as well as flush out of fine particulate material with increased risk for pathogen and organic micro-pollutant breakthrough. In addition, optimal expanded bed discharges debris, suspended solids and dirt and allows the individual GAC grains to collide and scrub each other, resulting in an increased filter life and performance capacity. Therefore, robust and flexible treatment processes require thorough design specifications and process control of backwash rates for filter cleaning. Since the GAC grains remain not constant, due to attrition, abrasive circumstances during backwashing and transport and due to biofilm layer growth on GAC grains, the fluidisation behaviour will change slowly but continuously. Engineers should be aware that prediction models have to be adjusted over time to cope with the process changes.

##### – Effect on operations

While it is possible to find a reasonably accurate voidage prediction model as a function of the fluid and particle properties, especially for individual GAC types, GAC is subject to change, and therefore it is most likely that the prediction accuracy will deteriorate rapidly. It is possible to fit a model for individual types of GAC, such as rock-like, rod-like and spherical particles with a considerably lower prediction error. Using advanced laboratory mea-

surements, accurate morphological properties of GAC can be obtained. Including these morphs into hydraulic models increases the prediction accuracy, but it also increases the complexity of the models. Finally, it can be concluded that the incipient voidage of GAC is significantly higher (0.50–0.65) than the commonly used voidage for solid granular materials (0.40).

## 5. Recommendations

To improve the GAC modelling and prediction accuracy, the following topics should be addressed:

- In full-scale filters, GAC must be re-activated and partly replaced by virgin GAC. Mixing of different types of GAC must be investigated on their overall expansion (and filtration) characteristics.
- A model needs to be developed that considers biofilm growth for applied GAC filtration.
- Highly spherical nylon balls have a similar density to wetted GAC. The expansion degree is very well known. This can be used to improve current knowledge about the fluidisation behaviour of GAC.
- When the expansion behaviour must be known, for instance when new sustainable GAC types are introduced, it is recommended to perform pilot plant experiments. If this is not an option, a considered prediction model can be used, but it is important to take a high degree of spread into account.
- This research focused on voidage and showed that the determination of the incipient voidage is rather complex. In many articles, the voidage is avoided by applying the degree of expansion. An alternative and more effective approach should be developed that makes it possible to predict the overall bed expansion for establishing optimal backwashing protocols.

## Declaration of Competing Interest

The authors declare that they have no known competing financial interests or personal relationships that could have appeared to influence the work reported in this paper.

## Acknowledgements

This research is part of the project entitled “Hydraulic modelling of liquid-solid fluidisation in drinking water treatment processes” carried out by Waternet, Delft University of Technology and HU University of Applied Sciences Utrecht. Financial support came from Waternet Drinking Water Production Department. For our simulation, we used Symbolic regression Software Eureqa. We thank Nutonian for allowing us to use their software.

We acknowledge and thank our students from Delft University of Technology, HU University of Applied Sciences Utrecht and Queen Mary University of London and in particular Fenne Philipse (Waternet) for the precise execution of many laboratory and pilot plant experiments. A special word of thanks goes to Ron Penners and Armand Middeldorp of Waterlab TU Delft. Finally, we also thank Clemy van der Steen-de Kok and Wim Oorthuizen (Dunea) as well as Ben Cools (de Watergroep) for the use of their Camsizers. Dr. Radomir Slavchov, we greatly appreciated your advice regarding the two-stage Washburn kinetics of capillary uptake.

This research project did not receive any specific grant from funding agencies in the public, commercial or not-for-profit sectors.

## Appendix A. Supplementary material

Raw data and additional information can be found in [55]. Supplementary data to this article can be found online at <https://doi.org/10.1016/j.appt.2021.06.017>.

## References

- [1] T.J. Bandosz, *Activated Carbon Surfaces in Environmental Remediation*, first ed., Academic Press, New York, 2006.
- [2] J.C. Crittenden, R.R. Trussell, D.W. Hand, K.J. Howe, G. Tchobanoglous, *MWH's Water Treatment: Principles and Design*, third ed., John Wiley & Sons, New York, 2012.
- [3] K.J. Howe, D.W. Hand, J.C. Crittenden, R. Rhodes Trussell, G. Tchobanoglous, *Principles of Water Treatment*, first ed., John Wiley & Sons Inc., New Jersey, 2012.
- [4] J.P. van der Hoek, J.A.M. Hofman, A.J. Graveland, The use of biological activated carbon filtration for the removal of natural organic matter and organic micropollutants from water, *Water Sci. Technol.* 40 (1999) 257–264, [https://doi.org/10.1016/S0273-1223\(99\)00664-2](https://doi.org/10.1016/S0273-1223(99)00664-2).
- [5] Th.G.J. Bosklopper, L.C. Rietveld, R. Babuska, B. Smaal, J. Timmer, Integrated operation of drinking water treatment plant at Amsterdam water supply, *Water Sci. Technol. Water Supply* 4 (2004) 263–270, <https://doi.org/10.2166/ws.2004.0116>.
- [6] L.C. Rietveld, Improving operation of drinking water treatment through modelling, 2005. <http://resolver.tudelft.nl/uuid:4f4e110a-a1ea-4d51-b645-3c9c58c67c92>.
- [7] J.R. Perrich, *Activated Carbon Adsorption for Wastewater Treatment*, first ed., CRC Press, New York, 1981, <http://www.copyright>.
- [8] R.C. Bansal, M. Goyal, *Activated Carbon Adsorption*, first ed., Taylor & Francis, 2005.
- [9] H. Marsh, F. Rodríguez-Reinoso, *Activated Carbon*, Elsevier Science & Technology Books, 2006.
- [10] S. Velten, Adsorption capacity and biological activity of biological activated carbon filters in drinking water treatment (2008), <https://doi.org/10.3929/ethz-a-005820821>.
- [11] F. Çeçen, O. Aktaş, *Activated Carbon for Water and Wastewater Treatment – Integration of Adsorption and Biological Treatment*, first ed., Wiley-VCH, Istanbul, 2010, <https://doi.org/10.1002/9783527628926>.
- [12] Z.K. Chowdhury, R.S. Summers, G.P. Westerhoff, B.J. Leto, K.O. Nowack, C.J. Corwin, L.B. Passantino, *The Authoritative Resource on Safe Water Solutions for Improving Water Quality Activated Carbon Solutions for Improving Water Quality*, first ed., American Water Works Association, Denver, 2012.
- [13] S.Y. Huncce, E. Soyer, Ö. Akgiray, On the backwash expansion of graded filter media, *Powder Technol.* 333 (2018) 262–268, <https://doi.org/10.1016/j.powtec.2018.04.032>.
- [14] C. Ray, R. Jain, *Drinking Water Treatment Focusing on Appropriate Technology and Sustainability Introduction*, first ed., Springer, Netherlands, Dordrecht, 2011, [https://doi.org/10.1007/978-94-007-1104-4\\_1](https://doi.org/10.1007/978-94-007-1104-4_1).
- [15] W.L. Filho, V. Sümer, *Sustainable Water Use and Management Examples of New Approaches and Perspectives*, first ed., Springer International Publishing, Cham, Switzerland, 2015, <https://doi.org/10.1007/978-3-319-12394-3>.
- [16] R.C. Marques, N.F. da Cruz, J. Pires, Measuring the sustainability of urban water services, *Environ. Sci. Policy* 54 (2015) 142–151, <https://doi.org/10.1016/j.envsci.2015.07.003>.
- [17] M. Naushad, E. Lichtfouse, *Environmental Chemistry for a Sustainable World – Green Materials for Wastewater Treatment*, Springer, 2020, <https://doi.org/10.1007/978-3-030-17724-9>.
- [18] J. Frank, A.S. Ruhl, Martin Jekel, Impacts of backwashing on granular activated carbon filters for advanced wastewater treatment, *Water Res.* 87 (2015) 166–174, <https://doi.org/10.1016/j.watres.2015.09.020>.
- [19] J. Kozeny, Über kapillare leitung des wassers im boden, *Akad. Wiss. Wien.* 136 (1927) 271–306.
- [20] P.C. Carman, Fluid flow through granular beds, *Trans., Inst. Chem. Eng.* 15 (1937) 32–48, [https://doi.org/10.1016/S0263-8762\(97\)80003-2](https://doi.org/10.1016/S0263-8762(97)80003-2).
- [21] S. Ergun, Fluid flow through packed columns, *Chem. Eng. Sci.* 48 (1952) 89–94.
- [22] J.F. Richardson, W.N. Zaki, Sedimentation and fluidisation: part I, *Trans. Inst. Chem. Eng.* 32 (1954) 35–53, [https://doi.org/10.1016/S0263-8762\(97\)80006-8](https://doi.org/10.1016/S0263-8762(97)80006-8).
- [23] W.C. van Lier, The influence of particle shape and particle size distribution on fluidisation behaviour of granular activated carbon in the aqueous phase, *Part. Part. Syst. Char.* 1 (1984) 143–152, <https://doi.org/10.1002/ppsc.19840010125>.
- [24] A. Akkoyunlu, Expansion of granular water filters during backwash, *Environ. Eng. Sci.* 20 (2003) 655–665, <https://doi.org/10.1089/109287503770736168>.
- [25] W. Dabrowski, M. Spaczyńska, R.I. Mackie, A model to predict granular activated carbon backwash curves, *Clean – Soil, Air, Water.* 36 (2008) 103–110, <https://doi.org/10.1002/clen.200600033>.
- [26] I. Sholji, Expansion of granular filters during backwashing, *J. Environ. Eng.* 113 (1987) 516–531.

- [27] R. Trussell, M. Chang, Review of flow through porous media as applied to head loss in water filters, *J. Environ. Eng.* 125 (1999) 998–1006.
- [28] M. Clements, J. Haarhoff, Practical experiences with granular activated carbon (GAC) at the Rietvlei water treatment plant, *Water SA* 30 (2004) 1–8. <http://www.wrc.org.za>.
- [29] A. Ujhidy, G. Bucsky, J. Németh, Hydrodynamic characteristics of activated carbon in air-and water-fluidized beds, *Korean J. Chem. Eng.* 25 (2008) 1170–1177.
- [30] S. Nikam, D. Mandal, A study on fluidization of activated carbon particles in gas-solid fluidized bed, *Indian Chem. Eng.* (2020) 1–13, <https://doi.org/10.1080/00194506.2020.1803149>.
- [31] G. Hoyland, General combined model for the hydrodynamic behaviour of fixed and fluidised granular beds, *Water Res.* 111 (2017) 163–176, <https://doi.org/10.1016/j.watres.2017.01.008>.
- [32] S.Y. Hunce, E. Soyer, Ö. Akgiray, Characterization of granular materials with internal pores for hydraulic calculations involving fixed and fluidized beds, *Ind. Eng. Chem. Res.* 55 (2016) 8636–8651, <https://doi.org/10.1021/acs.iecr.6b00953>.
- [33] J.T. Cornelissen, F. Taghipour, R. Escudí, N. Ellis, J.R. Grace, CFD modelling of a liquid-solid fluidized bed, *Chem. Eng. Sci.* 62 (2007) 6334–6348, <https://doi.org/10.1016/j.ces.2007.07.014>.
- [34] K. Zhang, G. Wu, S. Brandani, H. Chen, Y. Yang, CFD simulation of dynamic characteristics in liquid-solid fluidized beds, *Powder Technol.* 227 (2012) 104–110, <https://doi.org/10.1016/j.powtec.2012.01.030>.
- [35] R.W. Samstag, J.J. Ducoste, A. Griborio, I. Nopens, D.J. Batstone, J.D. Wicks, S. Saunders, E.A. Wicklein, G. Kenny, J. Laurent, CFD for wastewater treatment: an overview, *Water Sci. Technol.* 74 (2016) 549–563, <https://doi.org/10.2166/wst.2016.249>.
- [36] B. Blais, F. Bertrand, CFD-DEM investigation of viscous solid-liquid mixing: impact of particle properties and mixer characteristics, *Chem. Eng. Res. Des.* 118 (2017) 270–285, <https://doi.org/10.1016/j.cherd.2016.12.018>.
- [37] I. Mema, J.T. Padding, Fluidization of elongated particles – effect of multi-particle correlations for drag, lift, and torque in CFD-DEM, *AIChE J.* (2021) 1–11, <https://doi.org/10.1002/aic.17157>.
- [38] A. Cahyadi, S. Yang, J.W. Chew, CFD study on the hydrodynamics of fluidized granular activated carbon in AnFMBR applications, *Sep. Purif. Technol.* 178 (2017) 75–89, <https://doi.org/10.1016/j.seppur.2017.01.023>.
- [39] M. Clements, Granular activated carbon management at a water treatment plant, 2009. <http://hdl.handle.net/10210/2155> (accessed March 8, 2021).
- [40] O.J.I. Kramer, P.J. de Moel, J.T. Padding, E.T. Baars, S.B. Rutten, A.H.E. Elarbab, J.F. M. Hoof, E.S. Boek, J.P. van der Hoek, New hydraulic insights into rapid sand filter bed backwashing using the Carman-Kozeny model, *Water Res.* (2021).
- [41] K. Anderson, E. Chescattie, Incorporating filter bed expansion measurements into your backwashing routine, in: AWWA Water Quality Technology Conference, 2003.
- [42] E. Worch, Adsorption Technology in Water Treatment: Fundamentals, Processes, and Modeling, first ed., Walter de Gruyter GmbH & Co., Dresden, 2012.
- [43] A. Knezev, Microbial activity in granular activated carbon filters in drinking water treatment, 2015.
- [44] A.S. Pushnov, Calculation of average bed porosity, *Chem. Pet. Eng.* 42 (2006) 14–17.
- [45] Retsch-Technology, Operating instructions / Manual particle size analysis system: Camsizer, 2007.
- [46] A.M. Sereno, M.A. Silva, L. Mayor, Determination of particle density and porosity in foods and porous materials with high moisture content, *Int. J. Food Prop.* 10 (2007) 455–469, <https://doi.org/10.1080/10942910600880736>.
- [47] P.J. Sereda, R.F. Feldman, Wetting and drying of porous materials, *Canadian Build. Digest* 10 (1970) 1–7, <https://doi.org/10.4224/40000703>.
- [48] R.G. Peel, A. Benedek, C.M. Crowe, A branched pore kinetic model for activated carbon adsorption, *AIChE J.* 27 (1981) 26–32, <https://doi.org/10.1002/aic.690270106>.
- [49] B. Wolf, Application of hydrostatic weighing to density determination of tiny porous samples, *Rev. Sci. Instrum.* 66 (1995) 2578–2581, <https://doi.org/10.1063/1.1145591>.
- [50] B.M. Cummins, R. Chinthapatla, F.S. Ligler, G.M. Walker, Time-dependent model for fluid flow in porous materials with multiple pore sizes, *Anal. Chem.* 89 (2017) 4377–4381, <https://doi.org/10.1021/acs.analchem.6b04717>.
- [51] J.K. Edzwald, *Water Quality and Treatment: A Handbook on Drinking Water*, sixth ed., American Water Works Association, American Society of Civil Engineers, McGraw-Hill, New York, 2011.
- [52] J. van Keulen, Density of porous solids, *Mater. Struct.* 6 (1973) 181–183.
- [53] T. Ferreira, W. Rasband, ImageJ user guide, 2012. <https://doi.org/10.1038/nmeth.2019>.
- [54] Keyence, Digital microscope VHX-5000 user's manual, 2014.
- [55] O.J.I. Kramer, Dataset underlying the research of: new insights into the fluidisation characteristics of granular activated carbon for drinking water treatment applications, 4TU.ResearchData (2021), <https://doi.org/10.4121/14229863.v1>.
- [56] CEFIC, Test methods for activated carbon, Berlin, 1986. [https://activatedcarbon.org/images/Test\\_method\\_for\\_Activated\\_Carbon\\_86.pdf](https://activatedcarbon.org/images/Test_method_for_Activated_Carbon_86.pdf) (accessed March 8, 2021).
- [57] S. Davidson, M. Perkin, An investigation of density determination methods for porous materials, small samples and particulates, *Measurement: J. Int. Measurement Confed.* 46 (2013) 1766–1770, <https://doi.org/10.1016/j.measurement.2012.11.030>.
- [58] F.H.M. Nor, H. Othman, R.Z. Abidin, Density measurement of tridecane by using hydrostatic weighing system at density laboratory, NML-SIRIM, in: *Frontiers in Physics*, 3rd International Meeting, 2009 American Institute of Physics, 2009, pp. 196–202.
- [59] P.D.R. Dacomba Torres, Fluidization behavior of granular activated carbon: for drinking water treatment applications, 2018. <http://resolver.tudelft.nl/uuid:ea5e2d0c-76c5-4dd4-89b0-572ba3f71b80>.
- [60] A. Djerbi Tegger, Determining the water absorption of recycled aggregates utilizing hydrostatic weighing approach, *Constr. Build. Mater.* 27 (2012) 112–116, <https://doi.org/10.1016/j.conbuildmat.2011.08.018>.
- [61] A.G. Yiotis, I.N. Tsimpanogiannis, A.K. Stubos, Y.C. Yortsos, Coupling between external and internal mass transfer during drying of a porous medium, *Water Resour. Res.* 43 (2007) 1–12, <https://doi.org/10.1029/2006WR005558>.
- [62] A.S. Mujumdar, *Handbook of Industrial Drying*, fourth ed., CRC Press, 2006.
- [63] A.G. Yiotis, I.N. Tsimpanogiannis, A.K. Stubos, Y.C. Yortsos, Pore-network study of the characteristic periods in the drying of porous materials, *J. Colloid Interface Sci.* 297 (2006) 738–748, <https://doi.org/10.1016/j.jcis.2005.11.043>.
- [64] W.C. Yang, *Handbook of Fluidization and Fluid-Particle Systems*, first ed., CRC Press, New-York, 2003, [https://doi.org/10.1016/S1672-2515\(07\)60126-2](https://doi.org/10.1016/S1672-2515(07)60126-2).
- [65] E. Michaelide, C.T. Crowe, J.D. Schwarzkopf, *Multiphase Flow Handbook*, second ed., Taylor & Francis Inc, London, 2017.
- [66] O.J.I. Kramer, P.J. de Moel, J.T. Padding, E.T. Baars, Y.M.F. el Hasadi, E.S. Boek, J.P. van der Hoek, Accurate voidage prediction in fluidisation systems for full-scale drinking water pellet softening reactors using data driven models, *J. Water Process Eng.* 37 (2020) 1–15, <https://doi.org/10.1016/j.jwpe.2020.101481>.
- [67] O.J.I. Kramer, J.T. Padding, W.H. van Vugt, P.J. de Moel, E.T. Baars, E.S. Boek, J.P. van der Hoek, Improvement of voidage prediction in liquid-solid fluidized beds by inclusion of the Froude number in effective drag relations, *Int. J. Multiph. Flow* 127 (2020), <https://doi.org/10.1016/j.ijmultiphaseflow.2020.103261>.
- [68] R. Clift, J.R. Grace, M.E. Weber, *Bubbles, Drops, and Particles*, Academic Press, San Diego, CA, 1978.
- [69] A.H. Dharmarajah, Effect of particle shape on prediction of velocity-voidage relationship in fluidized solid-liquid systems, 1982.
- [70] T. Allen, *Particle Size Measurement – Powder Technology Series*, fourth ed., Chapman and Hall, London, 1990, <https://doi.org/10.1007/978-94-009-0417-0>.
- [71] R.G. Holdich, *Fundamentals of Particle Technology*, Midland Information Technology and Publishing, Leicestershire, 2002. <https://doi.org/10.4236/ns.2010.210132>.
- [72] E. Soyer, Ö. Akgiray, Expansion of non-spherical media during fluidization, in: *Proceedings of IWA International Conference on Particle Separation*, Seoul, South Korea, June 1–5, 2005, pp. 579–586.
- [73] H. Masuda, K. Higashitani, H. Yoshida, *Powder Technology: Fundamentals of Particles, Powder Beds, and Particle Generation*, CRC Press - Taylor & Francis Group, LLC., New York, 2007, <http://www.taylorandfrancis.com>.
- [74] M. Rhodes, *Introduction to Particle Technology*, second ed., John Wiley & Sons Ltd., Chichester, 2008, <https://doi.org/10.1002/9780470727102>.
- [75] J.S. Marshall, S. Li, *Adhesive Particle Flows*, Cambridge University Press, New York, 2014, <https://doi.org/10.1017/cbo9781139424547>.
- [76] J.P.K. Seville, C.Y. Yu, *Particle Technology and engineering, An Engineer's Guide to Particles and Powders: Fundamentals and Computational Approaches*, first ed., Butterworth-Heinemann, 2016.
- [77] A. Barroso-Bogeat, M. Alexandre-Franco, C. Fernández-González, V. Gómez-Serrano, Particle size distribution and morphological changes in activated carbon-metal oxide hybrid catalysts prepared under different heating conditions, *J. Microsc.* 261 (2016) 227–242, <https://doi.org/10.1111/jmi.12323>.
- [78] H. Wadell, Sphericity and roundness of rock particles, *J. Geol.* 41 (1933) 310–311, <https://doi.org/10.1086/624040>.
- [79] C.Y. Wen, Y.H. Yu, A generalized method for predicting the minimum fluidization velocity, *Am. Inst. Chem. Eng. J.* 12 (1966) 610–612, <https://doi.org/10.1002/aic.690120343>.
- [80] B.C. Lippens, J. Mulder, Prediction of the minimum fluidization velocity, *Powder Technol.* 75 (1993) 67–78, [https://doi.org/10.1016/0032-5910\(93\)80026-7](https://doi.org/10.1016/0032-5910(93)80026-7).
- [81] A. Anantharaman, R.A. Cocco, J.W. Chew, Evaluation of correlations for minimum fluidization velocity (Umf) in gas-solid fluidization, *Powder Technol.* 323 (2018) 454–485, <https://doi.org/10.1016/j.powtec.2017.10.016>.
- [82] J.R. Koza, Genetic programming: on the programming of computers by means of natural selection complex adaptive systems, 1992. [papers2://publication/uuid/5DADD85F-EE2F-42E1-8BF8-2CC6959C4FA0](https://pubs.opengroup.org/standards/5DADD85F-EE2F-42E1-8BF8-2CC6959C4FA0).
- [83] M.C. Mauguet, A. Montillet, J. Comiti, Macrostructural characterization of granular activated carbon beds, *J. Mater. Sci.* 40 (2005) 747–755, <https://doi.org/10.1007/s10853-005-6316-7>.
- [84] J. Rumble, *Handbook of Chemistry and Physics*, 101th ed., CRC Press, New York, 2019.
- [85] L.G. Gibilaro, *Fluidization-Dynamics, the Formulation and Applications of a Predictive Theory for the Fluidized State*, Butterworth-Heinemann, Oxford, 2001.
- [86] E.A. Shpirt, K.T. Alben, Changes in particle size distributions on a fixed bed of granular activated carbon, *Water Sci. Technol.* 18 (1986) 31–42. <https://iwaponline.com/wst/article-pdf/18/1/31/97336/31.pdf>.
- [87] V.R. Deitz, The heterogeneity of commercial granular activated carbons, *Carbon* 35 (1997) 579–584.